Nonisothermal Fusion Bonding in Semicrystalline Thermoplastics

Christopher J. G. Plummer, Pierre-Etienne Bourban, Jean-Emile Zanetto, Gregory D. Smith, Jan-Anders E. Månson

Laboratoire de Technologie des Composites et Polymères, Ecole Polytechnique Fédérale de Lausanne, CH-1015, Switzerland

Received 11 November 2001; accepted 16 May 2002

ABSTRACT: The development of the interfacial bond strength as a function of bonding conditions has been investigated in two representative semicrystalline thermoplastics, isotactic polypropylene and polyamide 12. If one side of the interface is well above the melting point immediately before contact, more rapid effective bonding is obtained for a given estimated interface temperature than under isothermal conditions. This is discussed in terms of a simple two-parameter model for the critical strain energy release rate associated with crack propagation along the interface, which incorporates the rate of establishment of intimate contact at the interface. The model provides a self-consistent phenomenological description of the time and temperature dependence of the bonding kinetics in polyamide 12 joints, although questions remain regarding the detailed mechanisms of bonding. © 2002 Wiley Periodicals, Inc. J Appl Polym Sci 87: 1267–1276, 2003

Key words: polyamides; poly(propylene) (PP); fracture; toughness

INTRODUCTION

Industrial fusion bonding falls into three broad classes, depending on whether the heat required to provoke melting at the interface is (1) introduced from an external source, (2) generated *in situ* by friction or radiation, or (3) available from a prior forming operation.[1–6] This last category is of particular relevance to integrated processing, currently under development in our laboratory for the production of multicomponent parts that combine the advantages of composites and neat resins.[7–9] The rational design of a sequence of forming operations will involve optimization of the total power consumption. Any heat (or mechanical work) introduced at a given stage of the process should, therefore, be exploited to the greatest possible extent during subsequent operations. If an injected component is to be fusion-bonded to a pre-existing component, for example, it may be advantageous to combine the two operations in a single overinjection step, rather than reheat the interface at a later stage. In the former case, joining occurs under nonisothermal conditions; that is, the surfaces to be joined are not at the same temperature immediately before contact.[7]

This provides the motivation for this study, which focuses on the specific problem of nonisothermal fusion bonding, as previously defined, by comparing experimental results for two representative systems and introducing a new phenomenological model for data interpolation. The model is then used to derive simple processing maps for the optimization of overinjection within an integrated process. In the experimental investigation, both nonisothermal fusion bonding and fusion bonding under isothermal conditions have been considered. The latter is of less relevance to integrated processing, but it provides a useful reference point when we consider nonisothermal bonding because isothermal bonding conditions are relatively well defined.[10–13] Moreover, it is hoped that such a comparison may further our understanding of the factors that dominate the development of joint strength in each case and, therefore, prepare the ground for controlled experimental studies of the underlying mechanisms.

In the past, fundamental studies of the thermally induced bonding of thermoplastics under well-defined conditions have tended to focus on amorphous systems and bonding temperatures just above the glass-transition temperature, T_g.[14–16] Such studies now often involve the characterization of the resistance to mode I crack propagation along the locus of the original interface with a linear elastic fracture mechanics (LEFM)-based test. The results are then expressed as a variation of the critical stress intensity factor, K_c, or the critical strain energy release rate, G_c, with the bonding time and temperature. It is usually

Correspondence to: J.-A. E. Månson (jan-anders.manson@epfl.ch).

Contract grant sponsor: Swiss Progamme Prioritaire en Matériaux.

© 2002 Wiley Periodicals, Inc.

possible to interpret this in terms of the establishment of strongly anchored covalent links across the interface. Thus, it has been shown that the development of strong joints between identical amorphous polymers held in contact at $T > T_g$ can be explained by the amount of self-diffusion necessary for entangled chains to straddle the interface.[14–20] One reason for the success of this approach is that as the polymer is cooled toward T_g, its self-diffusion coefficient becomes vanishingly small. Therefore, regardless of the importance of other processes (e.g., wetting and diffusion of contaminants away from the interface), experimental conditions can usually be chosen so that self-diffusion is the rate-controlling step. The bonding times under these conditions are generally too long to be of direct interest for industrial processing. However, such experiments have helped to establish the importance of entanglements in the mechanical properties of glassy polymers in general and the importance of well-anchored molecular connectors for good joint strength in particular.[21–24]

The same concepts now increasingly form the basis for discussions of semicrystalline polymers, and one might, therefore, anticipate similar considerations to apply to fusion bonding above the melting point, T_m. A direct dependence of G_c on the density of anchored covalent bonds across the interface, Σ, has been demonstrated for the diffusion-controlled reaction bonding of isotactic polypropylene (iPP) to polyamide 6 (PA6).[24–28] Moreover, it has been successfully modeled with a micromechanical approach[27] originally intended to describe crack propagation through a single craze in a glassy polymer.[29] This was justified in terms of the observation of single crazelike structures ahead of the crack tip. However, there is now evidence that the associated scaling of G_c with Σ^2 may be characteristic of other types of crack tip deformation zones, as long as deformation is localized to the crack tip.[28]

In the fusion bonding of identical (or miscible) semicrystalline polymers, chain diffusion may not be the rate-controlling step or at least not be the only rate-controlling process.[14] It is no longer possible to decrease the intrinsic melt self-diffusion constant indefinitely by a reduction in the bonding temperature because, in general, T_m is greater than T_g. Moreover, the assumption of a fully amorphous, homogeneous melt in initially semicrystalline polymers heated to temperatures up to, and even beyond, the equilibrium melting point, T_{m0}, is questionable, depending on the timescales under consideration. This leads to difficulties in modeling the thermorheological behavior. One can, therefore, neither assume nor discount models based on simple melt diffusion *a priori* in attempting to account for the kinetics of the formation of strong joints and their dependence on processing parameters.

EXPERIMENTAL

Specimen preparation

The two resins investigated were polyamide 12 (PA12) and iPP, both of which have been central to the development of integrated processing in our laboratory. However, they are also considered to be representative of other common semicrystalline thermoplastics. The PA12 was a commercial grade from Ems Chemie (Ems, Switzerland), with a molar mass of 16.4 kg/mol and a polydispersity of about 2. Differential scanning calorimetry heating scans of 5-mg samples at 10 K min^{-1} indicated the peak temperature of the melting endotherm of the as-received resin to be 178°C. The temperature defined in this way is denoted T_m. The iPP was a controlled rheology grade with a narrow molecular weight distribution,[11] supplied by Shell Chemicals (London, UK) in the form of extruded pellets, with a T_m value of 165°C. Fusion bonds were prepared from each material with injection-molded plaques (50 mm × 50 mm) around 2 mm thick.

Bonding

All the joints were prepared with an instrumented matched-die mold installed on a servohydraulic load frame.[10–13] The temperatures of the upper (T_1) and lower (T_2) halves of the mold were controlled separately and recorded as a function of time with thermocouples located on the upper and lower mold faces. A plaque was first placed in the upper mold. After T_1 and T_2 had stabilized to within 1 K of the required values, a second plaque was placed in the lower mold, and a thin polyimide strip was laid along one of its edges to provide a starter notch for fracture testing. The lower mold was covered with an insulating sheet, and the system was left to equilibrate for 10 min. The insulating sheet was then removed, the mold was closed, and a pressure p was applied. After the hold time, t_{hold}, the heaters were turned off, but p was maintained during subsequent cooling to 30°C. The initial cooling rate was about 55 K min^{-1} in each case.

For nonisothermal bonding with $T_1 \neq T_2$, the lower plaque was always hotter; that is, $T_1 < T_2$. The temperature of the interface, T_i, for the initial contact between the two plaques was estimated to be

$$T_i = (T_1 + T_2)/2 \quad (1)$$

This expression is only strictly valid for perfect contact between identical infinite plaques with constant heat capacity and thermal diffusivity. It has nevertheless been argued to be a useful approximation, based on detailed simulations considering the variations in the effective heat capacity with temperature and the effect of phase transformations.[11] The different test conditions investigated are summarized in Table I.

TABLE I
Processing Parameters for the Different Bonds ($\Delta T = T_2 - T_1$)

Series	T_1 (°C)	T_2 (°C)	t_{hold} (s)	p (MPa)	T_i (°C)	ΔT (°C)
PP1	100–160	100–160	600	2	100–160	0
PP2	100–160	200	42	2	150–180	100–401
PP3	140	200	0–600	2	170	60
PP4	140	200	40	0–40	170	60
PA1	170–210	170–210	60	2	170–210	2
PA2	160–170	190–230	60	2	180–200	40–60
PA3	180	180	60–1500	2	180	2
PA4	160	200	60–600	2	180	40
PA5	180	180	60	2–32	180	2
PA6	160	200	60	2–32	180	40

LEFM testing

For the characterization of the joint strengths, the mode I G_c value was measured with the double cantilever beam (DCB) geometry with a constant crack opening displacement (the wedge test), as illustrated in Figure 1. Bars (12 mm × 50 mm) were cut from the center of the bonded specimens. A crack was initiated by a wedge (a single-edged razorblade) being placed in the starter notch and by sufficient pressure being applied to induce pop-in at the interface.[11,12] Crack propagation was achieved by the wedge being pushed along the interface at a speed of 2 mm/min with a screw-driven load frame. The crack lengths on each side of the specimen were recorded with a video camera as functions of the position of the wedge, and the average crack length was determined from 8–10 separate measurements on a given specimen. Two specimens were tested for each set of bonding conditions, and G_c was determined with Kanninen's equation:[30]

$$G_c = \frac{3\Delta^2 E_1 h_1^3 E_2 h_2^3}{8a^4}\left[\frac{E_1 h_1^3 C_2^2 + E_2 h_2^3 C_1^2}{(E_1 h_1^3 C_2^3 + E_2 h_2^3 C_1^3)^2}\right] \quad (2)$$

where C_1 is $1 + 0.64h_1/a$, C_2 is $1 + 0.64h_2/a$, h_1 and h_2 are the heights of the beams on either side of the interface, Δ is the wedge thickness, and E_1 and E_2 are Young's moduli of the respective beams (Fig. 1). Although approximate, eq. (2) represents a substantial improvement over models based on simple classical beam theory[23] and is now widely used as a means of obtaining G_c data from DCB tests.[10–13,21,23–28,31,32] (Note that the scatter is relatively large for large G_c values because the experimentally determined quantity a is correspondingly small and increasingly difficult to determine precisely.) The loading time for the material in front of the advancing crack in these tests may be estimated as $\Delta t = a/\dot{a}$, where $\dot{a}$ is the crack propagation speed.[33] E was, therefore, determined from dynamic three-point bending tests at a frequency of $1/\Delta t \approx 0.01$ Hz. No significant changes in E were observed in any of the materials after bonding.

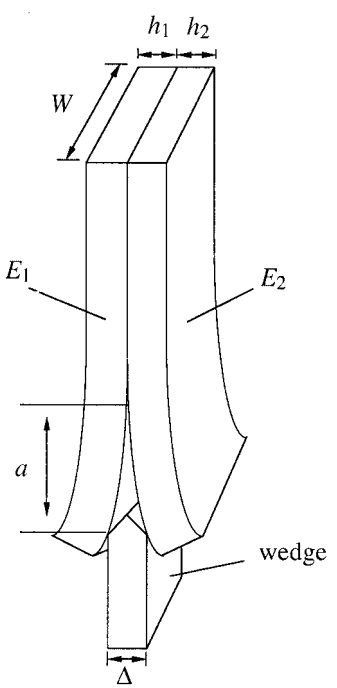

Figure 1 DCB test geometry with constant crack opening displacement.

RESULTS AND DISCUSSION

Figure 2 shows the results for PA12 and iPP joints prepared under isothermal and nonisothermal conditions. In each case, T_i was varied at constant t_{hold} and p values. For the nonisothermal bonding of PA12, $T_2 - T_1$ was maintained at 40 K, whereas for iPP, for reasons unconnected to this discussion, T_2 was maintained at 200°C and T_i was varied by variations in T_1. However, given that the results were relatively insensitive to the choice of T_2,[12,32] this was not expected to affect the comparative behavior of the two systems greatly. To facilitate the comparison, we have plotted G_c against $T_i - T_m$ in Figure 2. The behavior was indeed very similar for the two materials, although

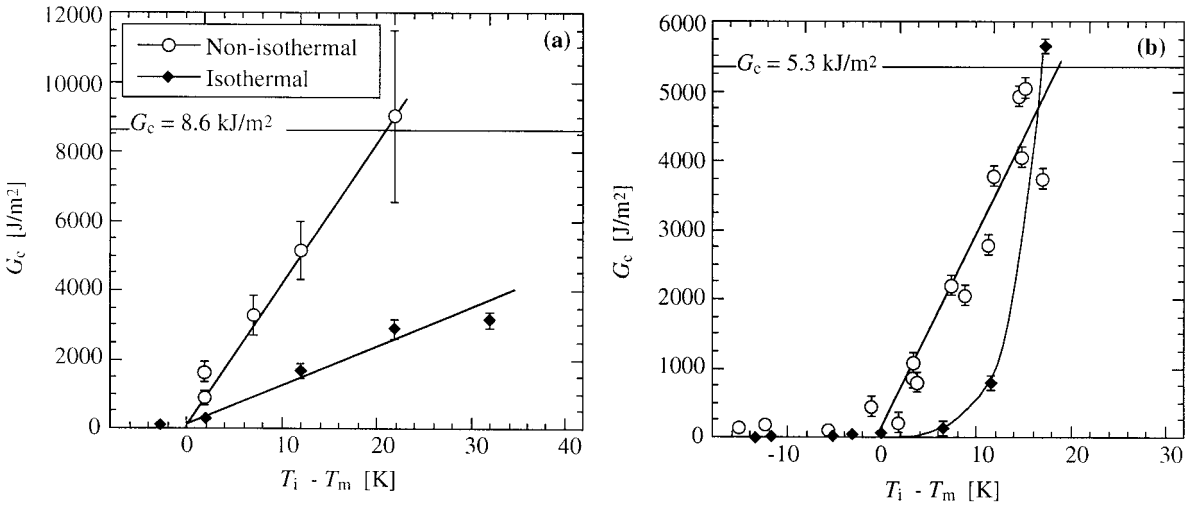

Figure 2 Bonding of PA12 and iPP under (♦) isothermal and (○) nonisothermal conditions for different $T_i - T_m$ values: (a) PA12 [series PA1 and PA2; t_{hold} = 60 s, p = 2 MPa, and $T_2 - T_1$ = 40 K (nonisothermal)] and (b) iPP [series PP1 and PP2; t_{hold} = 600 s (isothermal), t_{hold} = 42 s (nonisothermal), p = 2 MPa, and $T_2 - T_m$ = 35 K (nonisothermal)].

PA12 gave larger absolute values of G_c than iPP at large $T_i - T_m$ values, which was consistent with the higher G_c value observed for cohesive crack propagation in this material (G_c values for cohesive failure are also given in the figure). In each case, there was a monotonic rise in G_c with $T_i - T_m$ for $T_i - T_m > 0$. Moreover, over most of the range shown, nonisothermal conditions gave significantly stronger joints than isothermal conditions for a given value of $T_i - T_m$, and this occurred despite the substantially longer t_{hold} used for the isothermal bonding of iPP. Eventually, as $T_i - T_m$ was increased further, the results for the two types of bonding converged. This may be attributed to the lack of any further evolution in G_c once it reached the value for cohesive failure and, in the case of the nonisothermal bonding of iPP, where T_2 was fixed, a decrease in $T_2 - T_1$. Remarkably, the G_c value for cohesive failure was reached after less than a minute for the nonisothermal bonding of iPP with T_i only about 10 K above the nominal value of T_m.

The effect of t_{hold} for fixed values of other parameters is shown in Figure 3 for both nonisothermal and isothermal bonding in the case of PA12 and for nonisothermal bonding in the case of iPP. G_c tended toward its value for cohesive failure as t_{hold} increased, and for the conditions shown, the nonisothermal bonding of PA12 again gave higher G_c values than isothermal bonding for intermediate t_{hold}. In all cases, the t_{hold} value necessary to achieve cohesive strength increased markedly as $T_i - T_m$ tended to zero, and the strength of the PA12 joints prepared under isothermal conditions became negligible for all t_{hold} values inves-

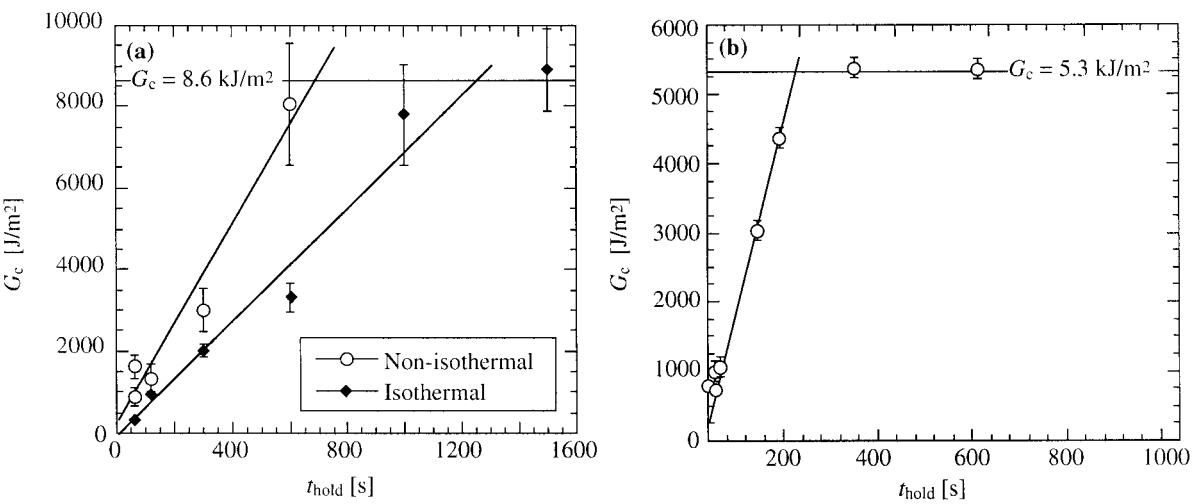

Figure 3 Bonding of PA12 and iPP under (♦) isothermal and (○) nonisothermal conditions for different t_{hold} values: (a) PA12 [series PA3 and PA4; $T_i - T_m$ = 2 K, p = 2 MPa, and $T_2 - T_m$ = 22 K (nonisothermal)] and (b) iPP [series PP3; $T_i - T_m$ = 5 K, p = 2 MPa, and $T_2 - T_m$ = 35 K (results given for nonisothermal bonding only)].

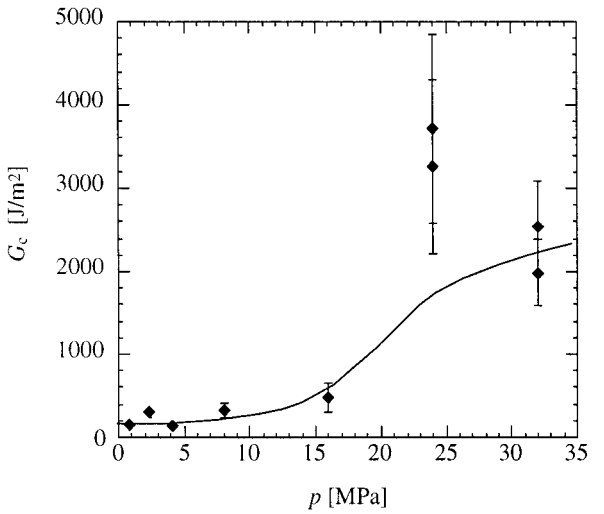

Figure 4 Bonding of PA12 under isothermal conditions for different p values (series PA5; t_{hold} = 60 s and $T_i - T_m$ = 2 K). The curve is a fit of the model for the evolution of G_c with p.

tigated. However, for the joints prepared under nonisothermal conditions, G_c values around 200 MPa $m^{1/2}$ were obtained with $T_i - T_m \leq 0$ in iPP. Moreover, these values were reached after very short t_{hold} values for the values of T_2 investigated here, as reflected by the apparently non-zero intercept of G_c plotted against t_{hold} in Figure 3.

The effect of p on the isothermal bonding of PA12 is shown in Figure 4. G_c increased significantly with p, but this increase was most noticeable in the range 15 MPa $< p <$ 25 MPa, beyond which G_c showed little further change (although the combination of large p values and relatively low T_i values led to relatively inhomogeneous wetting and correspondingly large scatter in the results). For nonisothermal bonding, however, there was an intermediate range of p in which G_c decreased sharply as p increased, as shown in Figure 5. These trends may be explained in terms of the establishment of intimate contact and wetting at the interface during bonding. As well as being prerequisites for self-diffusion across the interface, effective contact and wetting should maximize the contributions of van der Waals and other secondary interactions to adhesion and promote physical interlocking. For interfaces between solid or partially solid rough surfaces, this requires smoothing out or filling in the surface roughness.[34] Therefore, for isothermal bonding with nominal T_i values less than or around T_m, one anticipates an increase in the effective contact area at fixed t_{hold} and T_i values as p is increased,[34–37] which is consistent with the results in Figure 4. For PA12, relatively high p values were necessary to improve G_c significantly under these conditions, but the observation that G_c reached a nearly constant value at the highest p value suggests full contact was eventually achieved. That G_c remained less than for cohesive failure in PA12 in this latter regime nevertheless indicated t_{hold} = 60 s to be insufficient for complete healing of the interface.

This interpretation is also consistent with the observation of relatively strong joints for nonisothermal bonding. Because the temperature of the hotter plaque was well above T_m in both the PA12 and iPP joints, the establishment of intimate contact was expected to be rapid for all p values. This is illustrated by Figure 3, which shows the bonding of PA12 under nonisothermal conditions with a T_i value 22 K above T_m, which leads to a G_c value close to the value for cohesive failure for t_{hold} = 60 s and p = 2 MPa. T_m is itself an increasing function of p, as shown in Figure 5. This would not have affected the melting of the hotter plaque because it was always molten before the clo-

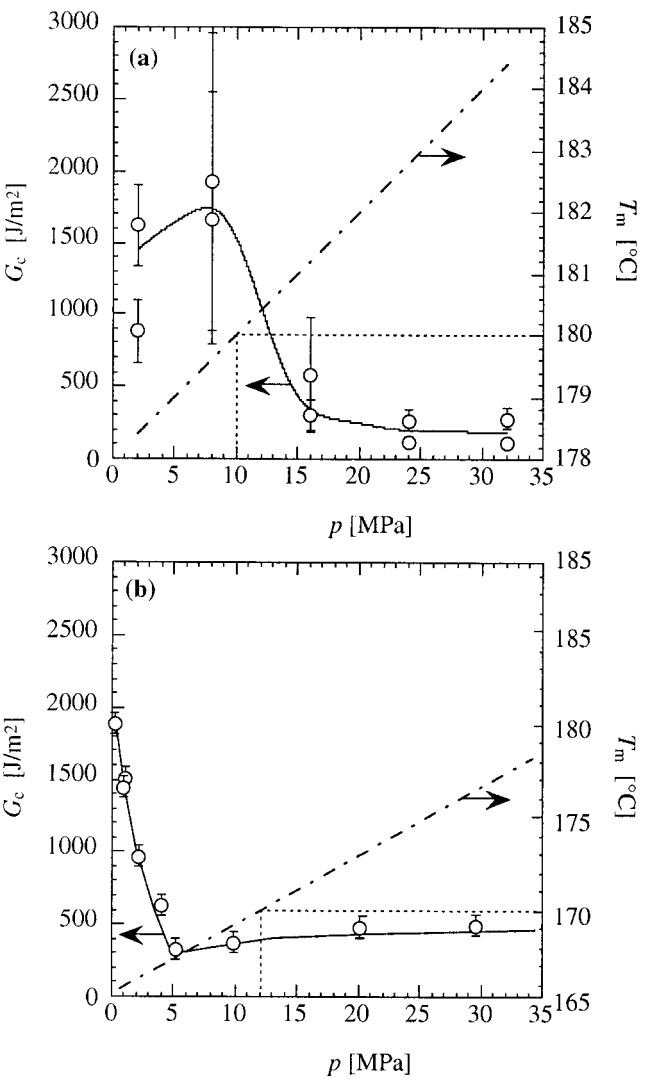

Figure 5 Effect of p on the nonisothermal bonding of PA12 and iPP: (a) PA12 (series PA6; t_{hold} = 60 s, $T_i - T_m$ = 2 K, and $T_2 - T_m$ = 22 K) and (b) iPP (series PP4; t_{hold} = 42 s, $T_i - T_m$ = 5 K, and $T_2 - T_m$ = 35 K).

sure of the mold. However, because T_m increases with respect to T_i as p is raised, a decrease in interdiffusion and, therefore, a decrease in G_c are expected at sufficiently high p values on account of the suppression of melting at the surface of the colder plaque. For PA12 under the conditions of Figure 5, T_m became approximately equal to T_i when p reached 10 MPa, and this is consistent with the observed decrease in G_c for $p > 10$ MPa. The G_c values at the highest p value might, therefore, be attributed to secondary interactions alone, although it is not clear to what extent the applied pressure could be considered effective at the instant of contact. G_c in this regime was nevertheless comparable to the G_c values obtained for nonisothermal bonding with $T_i - T_m \leq 0$ and for which a substantial degree of contact may be assumed, given that T_2 was always well above T_m.

In summary, the marked differences between the results for isothermal and nonisothermal bonding and the sensitivity of the bond strengths to the applied pressure strongly suggest the establishment of intimate physical contact at the interface, through the smoothing out of surface asperities, for example, to be a significant factor in the bonding kinetics. In the most general case, the evolution of joint strength during fusion bonding will involve both the rate of establishment of intimate contact at the interface, dX/dt, and some function $D(t)$ that describes the evolution of the bond strength once contact is achieved locally. $G_c(t)$ can then be written as a convolution:[35–37]

$$G_c(t) = \int_0^t \frac{dX}{d\xi} D(t - \xi)\, d\xi \qquad (3)$$

Although $D(t)$ may be linked at least indirectly with diffusion processes,[37] in view of the possible influence on the wetting behavior of factors such as contamination or oxidation at the interface and the potentially complex thermorheological behavior at temperatures close to T_m, it is difficult to justify detailed assumptions concerning its form *a priori*. Indeed, estimates of the reptation times for PA12 samples of molecular weights similar to that used here, based on rheological data for homogeneous melts, suggest that interdiffusion at the interface should be relatively rapid in the temperature range investigated.[32] Therefore, either diffusion is not a rate-controlling factor or simple first-principle calculations of the reptation time in a homogeneous melt are inadequate in this context. It might nevertheless be possible to infer $D(t,T_i)$ directly from the dependence of G_c on t_{hold} for T_2 values sufficiently high for the establishment of contact no longer to be rate-controlling. This is of particular interest in that it would imply (1) the suitability of nonisothermal bonding for the investigation of the microscopic bonding mechanisms and (2) the possibility of separating the different contributions to the kinetics of isothermal bonding by a comparison of the data with those obtained from nonisothermal bonding at the same value of T_i.

Simplified model for the establishment of intimate contact during isothermal bonding

As a basis for further discussion, a simplified model for the establishment of intimate contact is introduced. Regions of contact are assumed to initiate from a number of points per unit area of the interface, α, whose number depends on time in the most general case, and to grow at some rate $\dot{r}$, which may also depend on time. If all the regions grow at the same rate, this is described by[38–42]

$$X(t) = 1 - \exp\left[-k \int_0^t \alpha(\zeta)\left(\int_\zeta^t \dot{r}(\xi)\, d\xi\right)^m d\zeta\right] \qquad (4)$$

where $X(t)$ is the relative contact area after time t and k and m depend on the geometry of the growing entities (e.g., $k = \pi$ and $m = 2$ for circular contacts).

The contact area is assumed to increase via the squeezing flow of a non-Newtonian fluid (the melt) under the influence of a constant global pressure p. For pure extensional flow or mixed-shear extensional flow of asperities with initially triangular cross sections,[43]

$$\dot{r} \approx r\rho^2 \dot{\varepsilon}_o \left(\frac{p_x}{p_o}\right)^n$$

where $\dot{\varepsilon}$ and p_o are constant for a fixed temperature, ρ is the effective aspect ratio of the asperities, and

$$p_x = \frac{p}{X}$$

$\dot{\varepsilon}_o$ and p_o are constant for a fixed temperature, ρ is the effective aspect ratio of the asperities, and p_X is equal to p/X. In this geometry, the effective volume of material being squeezed at the interface is roughly proportional to r, so similar scaling is also anticipated for pure shear flow (whereas for a shear flow of constant volume elements, $\dot{r}$ decreases with r[37]). Because $\dot{r}$ depends on r, the use of eq. (4) imposes the assumption of a constant number of points of contact per unit area of the interface, α_o, established instantaneously at $t = 0$, so that

$$X(t) = 1 - \exp\left[-k\rho^{2m}\dot{\varepsilon}_o^m \left(\frac{p}{p_o}\right)^{nm} \alpha_o \left(\int_0^t r(\xi)X(\xi)^{-n}\, d\xi\right)^m\right]$$

(no attempt has been made to consider the effect of the coalescence of the growing regions on $\dot{r}$). In this case, ridged contact surfaces are observed,[10–12,32] and a one-dimensional form of eq. (4) is, therefore, considered most appropriate:

$$X(t) = 1 - \exp\left[-2\rho^2\dot{\varepsilon}_o\left(\frac{p}{p_o}\right)^n \alpha_o \int_0^t r(\xi)X(\xi)^{-n}\,d\xi\right] \quad (5)$$

Noting that

$$X(r) = 1 - \exp[-2\alpha_0 r]$$

we may rewrite eq. (5) as follows:

$$X(t^*) = 1 - \exp\left\{-\int_0^{t^*} - \ln[1 - X(\xi)]X(\xi)^{-n}\,d\xi\right\} \quad (6)$$

$$t^* = \frac{t}{\tau_1} \text{ and } \tau_1 = \rho^{-2}\dot{\varepsilon}_o^{-1}\left(\frac{p_o}{p}\right)^n$$

where ρ is the mean height-to-width ratio of the ridges.

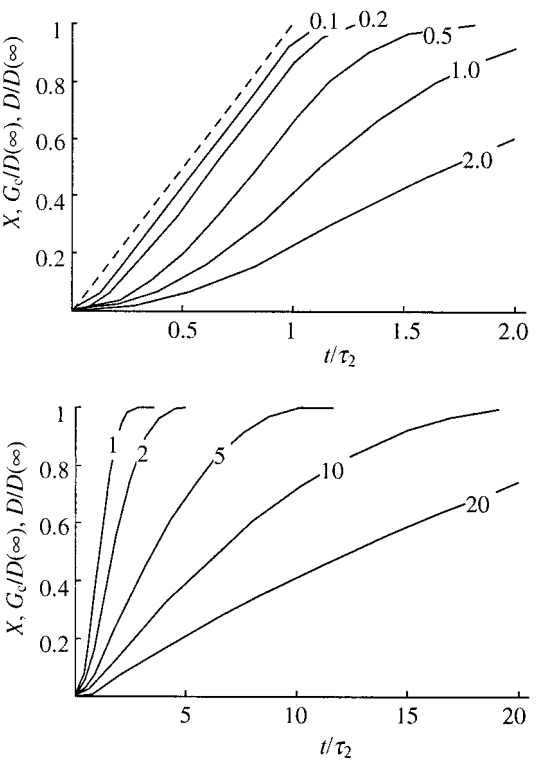

Figure 6 Predicted $G_c/D(\infty)$ and D (dotted line) values for a constant value of τ_2 plotted as a function of t/τ_2 for different τ_1/τ_2 values as indicated (two different sets of axes are given for clarity).

Comparison with the data

For the polyamides, $n \approx 1$, so the characteristic time for the establishment of contact may be rewritten:

$$\tau_1 \approx \frac{\mu}{\rho^2 p} \quad (7)$$

where μ is the effective viscosity. The differential form of eq. (6) is then

$$\frac{dX}{dt^*} = \frac{X - 1}{X}\ln(1 - X)$$

for which

$$X \approx t^* - \frac{t^{*2}}{4},\ t^* \le 2$$

$$X \approx 1,\ t^* > 2 \quad (8)$$

is an approximate solution. If $D(t)$ is now assumed to be given approximately by

$$\frac{D(t)}{D(\infty)} = \frac{t}{\tau_2} = \frac{\tau_1}{\tau_2}t^*,\ t \le \tau_2$$

$$D(t) = D(\infty),\ t > \tau_2 \quad (9)$$

straightforward analytical expressions for G_c may be obtained from eq. (3). The resulting forms of X and $G_c/D(\infty)$ are shown in Figure 6 as functions of t/τ_2 for different values of τ_1/τ_2 and for constant τ_2.

For $T_i - T_m = 2$ K, τ_2 is estimated directly from the data in Figure 4 to be 150 s, with D assumed to be independent of p and with G_c tending to about 0.4 times its value for cohesive failure in the limit of very large p ($\tau_2 \gg \tau_1$). The pressure dependence of G_c is derived from eq. (7), which may be rewritten as follows:

$$\tau_1 = \frac{A}{p}$$

An approximate fit to the data is given in Figure 4 with $\tau_2 = 150$ s and $A = 1200$ MPa s. The data suggested a far more pronounced sigmoidal shape for $G_c(p)$ than predicted, and it was necessary to assume a non-zero initial degree of contact, that is, $X(t = 0) > 0$, to account for the data at low p. The discrepancies may reflect both the quality of the data and the approximations inherent in the model. They could be due, for example, to an increase in the number of individual contacts with time, which would lead to an effective time delay in the onset of relatively rapid bonding. The predicted evolution of G_c with t for $T_i - T_m = 2$ K

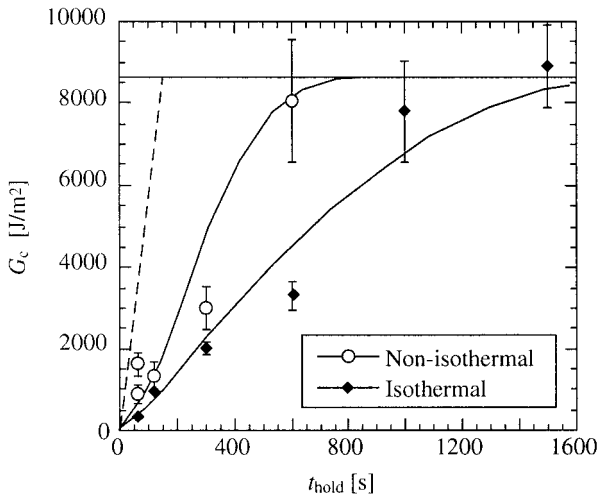

Figure 7 Comparison of the isothermal and nonisothermal data given in Figure 3 with the predictions of the model [D(∞) = 8.6 kJ/m^2, τ_2 = 150 s, τ_1 = 240 s (nonisothermal data), and τ_1 = 600 s (isothermal data)].

and p = 2 MPa, with A = 1200 MPa s and τ_2 = 150 s, was consistent with the isothermal data, as shown in Figure 7, but the data again suggested a more sigmoidal shape for $G_c(t)$ than predicted by the model.

In the nonisothermal case, D was taken to depend only on T_i because T_i has been assumed to reach values close to T_i as soon as intimate contact is established locally. For the conditions of Figure 2, τ_2 = 150 s also implied a significant contribution to the nonisothermal bonding kinetics from the establishment of contact, as suggested by Figure 7. Therefore, on the basis of the observed pressure dependence of G_c, $T_2 - T_m$ = 22 K did not appear to be sufficient for the direct separation of the contributions of D and X to bonding to be possible by a comparison of the isothermal and nonisothermal data at p = 2 MPa. Essentially the same conclusions were reached based on other reasonable choices of the form of D, such as the $t^{1/2}$ dependence observed in glassy polymers.[14–16]

If it is now supposed that the effective temperature during the establishment of contact in nonisothermal bonding is constant, the rate equation should take the same form as in the isothermal case. This is clearly not a very realistic assumption, given that large time-dependent temperature gradients are close to the interface once contact has occurred locally, and μ in eq. (7) will, therefore, not generally be time-independent (a time-dependent μ value could be included in eq. (4), but detailed modeling of the local coupling between viscous flow and heat flow has not been attempted). The fit to the nonisothermal data shown in Figure 7 implies τ_1 = 240 s, whereas τ_1 is estimated to be 600 s for the isothermal data. From the nonisothermal data in Figure 2, for $T_i - T_m$ = 22 K, $\tau_2 \leq$ 60 s. If τ_1 = 240 s and τ_2 = 60 s are used to predict G_c for t_{hold} = 60 s and $T_i - T_m = T_2 - T_m$ = 22 K, a value of about 1500 J/m^2 is obtained, which is somewhat less than the observed value (see Fig. 3). This is not surprising because it is reasonable to expect the effective temperature during the establishment of contact in the nonisothermal case to be less than T_2.

Despite these limitations, this approach is thought to provide a working two-parameter description of the bonding process that is consistent with the observed behavior. The question of the physical origin of the inferred values of τ_1 and τ_2 is not clear, however. Because both these quantities are implicitly assumed to tend to infinity as T tends to T_m, they cannot be consistent with estimates of quantities such as the diffusion constant (as discussed earlier) or the viscosity from the homogeneous melt. Indeed, estimates based on the melt viscosity severely underestimate τ_1. For example, the (linear) shear viscosity, η_o, of PA12 of a comparable molecular weight measured after the cooling of a fully molten sample to T_m + 2 is around 10^3 Pa s.[32] Therefore, for p = 2 MPa and $\rho \sim 0.02$ (from profilometry measurements[32]) and $\mu = 3\eta_o$ (for extensional flow), τ_1 is estimated from eq. (7) to be about 3 s. Similar estimates for the characteristic time are also predicted by other approaches[37] with the same value of η_o and the same profilometry data.[32]

Given that the establishment of contact does not depend on the absolute size of the asperities at the contact surfaces according to this model, it would be of great interest to investigate the contact behavior at model interfaces with well-defined macroscopic roughness. However, even given a realistic model for this aspect of the bonding process, it should be borne in mind that G_c and the local mode mixity may depend not only on the microscopic state of the interface but also on the surrounding microstructure, as discussed in detail elsewhere.[10–12,32] This microstructure is clearly sensitive to the flow history, particularly for bonding temperatures just above T_m, where extensional flow may contribute to enhanced crystallization rates, further complicating the rheological behavior. Moreover, the asymmetry in the structure close to the interface may lead to local departures from the stress states implicitly assumed in the calculation of G_c, with consequences both for the microdeformation behavior and for the macroscopically determined values of G_c.[12]

Simple interpolation-based processing maps

One of our main aims is to use the analytical descriptions of the bonding process introduced in the preceding sections to sketch the form for G_c over the full range of T_i and t_{hold} values investigated. This allows us to construct simple processing diagrams for the bonding of PA12, which provide a useful summary of the effects of these processing parameters. Examples are shown for PA12 under isothermal and nonisother-

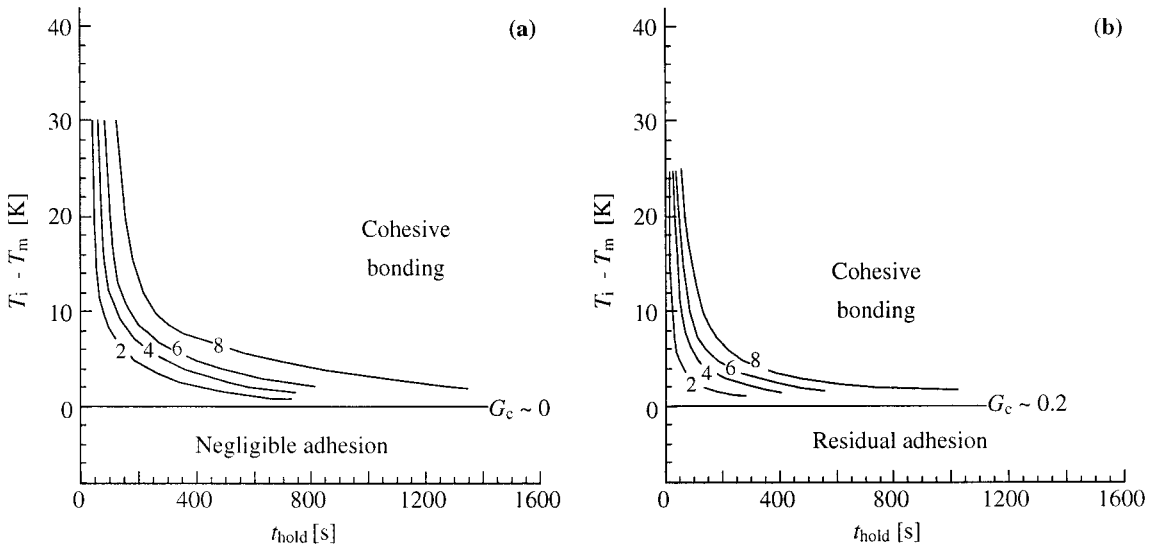

Figure 8 Processing maps for PA12 joints and $p = 2$ MPa obtained with the data given in Figures 2 and 3 for estimating the contours of a constant value of G_c under (a) isothermal conditions and (b) nonisothermal conditions ($T_2 - T_1 = 40$ K).

mal conditions with $p = 2$ MPa in Figure 8, in which the contours of constant G_c have been plotted in $\{t_{hold}, T_i - T_m\}$ space. In each case, τ_1 and τ_2 were estimated with a power law of the form $B(T - T_m)^\gamma$ to interpolate the values inferred directly from fits to the data. This procedure may be extended to construct constant G_c surfaces in $\{t_{hold}, T_i - T_m, T_2 - T_m\}$ space, but the essential features of the behavior are already apparent in Figure 8. It would also be of practical interest to include the locus of the onset of significant thermal degradation in such diagrams, but in this case, no significant bulk thermal degradation was detected in the range of conditions shown.[32] Similar processing diagrams have also been derived from the data for iPP.[11]

CONCLUSIONS

For estimated T_i's just above T_m, nonisothermal bonding between solid plaques and plaques initially at temperatures well above T_m has been shown to result in bonds with G_c approaching that of the bulk resins after much shorter times than for isothermal bonding at the same T_i values. Moreover, even for T_i's below T_m, nonisothermal bonding resulted in residual adhesive strength, whereas isothermal bonding gave negligible adhesion. Therefore, although our interest in nonisothermal bonding stems mainly from its relevance to multistep processing, this work suggests that it may be intrinsically advantageous with respect to isothermal bonding in terms of processing times and temperatures.

It is inferred from these differences in isothermal and nonisothermal bonding and the pressure sensitivity of the bond strength that one of the most important factors is the establishment of intimate physical contact and wetting at the interface. On this basis, a simple phenomenological model has been proposed to account for the experimental results and, therefore, to construct processing windows defining the range of parameters for which useful bond strengths can be obtained. This has fulfilled the aim of developing guidelines for the optimization of nonisothermal bonding in an integrated process. In the case of PA12, the processing windows show that considerable freedom in the choice of bonding temperatures is possible because the degradation of the polymer does not occur until much higher temperatures or longer times than those required for bonding.[32] This may not be the case for more heat-sensitive resins, but the method used here can easily be adapted to these by the incorporation of information on the degradation behavior.

A detailed physical description of the empirically determined characteristic times for the establishment of contact and the development of bond strength once intimate contact has been achieved is nevertheless lacking. One difficulty with assuming these to be simply related to local microscopic processes such as diffusion across the interface is that only G_c is directly accessible with this experimental approach. Microscopic observations, however, indicate the microdeformation processes at the interface to be relatively complex.[10–12,32] They are highly dependent on the microstructure not only at but also in the immediate vicinity of the interface, which is, in turn, strongly dependent on the thermal history. Further progress may, therefore, necessitate both the generation of data for a wider range of conditions and a more systematic investigation of the role of the microstructure, the effect of the interface geometry on the establishment of contact, and the effective viscosity of the melt in the temperature range of interest.

The authors acknowledge H.-H. Kausch for helpful discussions.

References

1. Benatar, A.; Gutowski, T. G. SAMPE J 1986, 19, 33.
2. Grimm, R. A. Welding J 1990, 3, 23.
3. Grimm, R. A. Adv Mater Process 1995, 3, 27.
4. Potente, H.; Natrop, J.; Pederson, T. K.; Uebbing, M. J Thermoplast Compos 1993, 6, 147.
5. von der Ohn, J. Welding Int 1990, 4, 288.
6. Weber, J. Welding J 1990, 69, 52.
7. Bourban, P.-E.; Smith, G. D.; Bonjour, F.; Månson, J.-A. E. Proceedings of the 16th International SAMPE: Niederglatt, Switzerland, Lang, R. W.; Erath, M. A., Eds. May 30 to June 1, 1995; p 305.
8. Bourban, P. E.; Bonjour, F.; Månson, J.-A. E. Proceedings of ECCM7, Woodhead: Cambridge, UK, May 14–16, 1996; p 201.
9. Bourban, P.-E.; Bögli, A.; Bonjour, F.; Månson, J.-A. E. Compos Sci Technol 1997, 58, 633.
10. Smith, G. D.; Plummer, C. J. G.; Bourban, P.-E.; Månson, J.-A. E. Polymer 2001, 42, 6247.
11. Smith, G. D. Ph.D. Thesis, Ecole Polytechnique Fédérale de Lausanne, 1997.
12. Zanetto, J.-E.; Plummer, C. J. G.; Bourban, P.-E.; Månson, J.-E. A. Polym Eng Sci 2001, 41, 890.
13. Smith, G. D.; Toll, S.; Månson, J.-A. E. Proceedings of the 3rd International Conference on Flow Processes in Composite Materials, University College Galway: Galway, Ireland, July 7–9, 1994; p 423.
14. Kausch, H.-H. Polymer Fracture, 2nd ed.; Springer: Heidelberg, 1987.
15. Jud, K.; Kausch, H.-H. Polym Bull 1979, 1, 697.
16. Jud, K.; Kausch, H.-H.; Williams, J. G. J Mater Sci 1981, 16, 204.
17. DeGennes, P. G. C R Acad Sci Paris Ser B 1980, 291, 219.
18. Prager, S.; Tirrell, M. J Chem Phys 1981, 73, 5194.
19. Kim, Y. H.; Wool, R. P. Macromolecules 1983, 16, 1115.
20. Wool, R. P.; O'Connor, K. M. J Appl Phys 1981, 52, 5953.
21. Char, K.; Brown, H. R.; Deline, V. R. Macromolecules 1993, 26, 4164.
22. Brown, H. R.; Char, K.; Deline, V. R.; Green, P. F. Macromolecules 1993, 26, 4155.
23. Creton, C.; Kramer, E. J.; Hui, C.-Y.; Brown, H. R. Macromolecules 1992, 25, 3075.
24. Creton, C.; Kramer, E. J.; Brown, H. R.; Hui, C.-Y. Adv Polym Sci 2002, 53, 156.
25. Boucher, E.; Folkers, J. P. ; Hervet, H.; Leger, L.; Creton, C. Macromolecules 1996, 29, 774.
26. Boucher, E.; Folkers, J. P.; Creton, C.; Hervet, H.; Léger, L. Macromolecules 1997, 30, 2102.
27. Plummer, C. J. G.; Creton, C.; Kalb, F.; Léger, L. Macromolecules 1998, 31, 6164.
28. Kalb, F.; Léger, L.; Plummer, C. J. G.; Creton, C.; Marcus, P. Macromolecules 2000, 34, 2702.
29. Brown, H. R. Macromolecules 1991, 24, 2752.
30. Kanninen, M. F. Int J Fract 1973, 9, 83
31. Bideaux, J.-E.; Smith, G. D.; Månson, J.-A. E.; Plummer, C. J. G.; Hilborn, J. G. Polymer 1998, 39, 5953.
32. Zanetto, J.-E. Ph.D. Thesis, Ecole Polytechnique Fédérale de Lausanne, 2000.
33. DeGennes, P. G. C R Acad Sci Paris Ser B 1988, 307, 1949.
34. Karakazov, E. S. Welding Prod 1976, 23, 2.
35. Mantell, S. C.; Springer, G. S. J Compos Mater 1992, 26, 2348.
36. Lee, W. I.; Springer, G. S. J Compos Mater 1987, 21, 1017.
37. Butler, C. A.; McCullough, R.; Pitchumani, R.; Gillespie, J. W. J. J Thermoplast Compos Mater 1998, 11, 338.
38. Avrami, M. J. J Chem Phys 1941, 9, 177.
39. Avrami, M. J. J Chem Phys 1940, 8, 212.
40. Avrami, M. J. J Chem Phys 1939, 7, 1103.
41. Kolmogoroff, A. N. Izv Akad Nauk Ser Math 1937, 3, 335.
42. Evans, U. R. Trans Faraday Soc 1945, 41, 365.
43. Tanner, R. I. Engineering Rheology, 2nd ed.; Oxford University Press: Oxford, 2000.